Received April 14, 2019, accepted May 5, 2019, date of publication May 22, 2019, date of current version June 6, 2019.

Digital Object Identifier 10.1109/ACCESS.2019.2918345

Power Control for Clustering Car-Following V2X Communication System With Non-Orthogonal Multiple Access

HAILIN XIAO[1,2], (Member, IEEE), YUHONG CHEN[2], SHAN OUYANG[3], (Senior Member, IEEE), AND ANTHONY THEODORE CHRONOPOULOS[4,5], (Senior Member, IEEE)

[1]School of Computer Science and Information Engineering, Hubei University, 430062, China
[2]Key Laboratory of Cognitive Radio and Information Processing, Ministry of Education, Guilin University of Electronic Technology, Guilin 541004, China
[3]Guangxi Key Laboratory of Wireless Wideband Communication and Signal Processing, Guilin University of Electronic Technology, Guilin 541004, China
[4]Department of Computer Science, The University of Texas at San Antonio, San Antonio, TX 78249, USA
[5]Department of Computer Engineering and Informatics, University of Patras, 26500 Patras, Greece

Corresponding author: Hailin Xiao (xhl_xiaohailin@163.com)

This work was supported in part by the National Natural Science Foundation of China under Grant 61872406 and Grant 61472094, and in part by the Key Research and Development Plan Project of Zhejiang Province under Grant 2018C01059.

ABSTRACT Vehicle clustering has been utilized for reducing the complexity of vehicle-to-everything (V2X) communications that would ultimately improve road traffic efficiency. Using a car-following model in a V2X communication system, we propose a vehicle clustering method for dynamically classifying vehicles and adjusting cluster size in real time. The especially important issue for the selected cluster-head vehicles (CHVs) can achieve an optimal trade-off between the CHVs' relative speed and power allocation. Furthermore, in order to balance the power allocation among the CHVs to further increase the downlink throughput, a power control approach for non-orthogonal multiple access (NOMA) is proposed. In this approach, the power allocation coefficients are obtained by maximizing the achievable rate while meeting the predefined target rate of each NOMA user. Finally, numerical simulations are provided to confirm the theoretical results and demonstrate the superior performance of the proposed approach. Note that through the numerical simulations, we can find the critical point of maximizing the minimum achievable rate among the CHVs at low transmission power of base station (BS).

INDEX TERMS Power allocation, non-orthogonal multiple access, vehicular networks, cooperative communication, vehicle-to-everything communications.

I. INTRODUCTION

Recently, vehicle-to-everything (V2X) communications have attracted widespread attention in academia and industry for their providing more efficient, smarter, and safer road traffic [1]–[3]. V2X communications typically include vehicle-to-vehicle (V2V), vehicle-to-infrastructure (V2I) and vehicle-to-pedestrian (V2P) transmissions to enable real-time traffic information exchange among vehicles, pedestrians and infrastructure [4]–[6]. The main present challenge in developing V2X communications is to address the issues of severe data congestion and low access efficiency caused by the ever-increasing number of connected vehicles in vehicular networks [7], [8]. Non-orthogonal multiple access (NOMA) is a promising technique for the fifth-generation (5G) wireless systems, which not only meets growing traffic requirements but also enables large-scale device connectivity [9]–[11]. Therefore, the combination of NOMA technology in vehicular networks enables multiple vehicles to simultaneously transmit information on the same channel, thereby alleviating the resource conflicts such as limited transmission capacity and unpredictable propagation delays in V2X communications [12], [13].

It is well known that the vehicular networks are dynamic due to the real-time change of road traffic, thereby inevitably bringing about the problem of unstable network topology [14]–[16]. However, a clustering method has been proposed that makes the network topology hierarchical and scalable by establishing a connectivity graph between vehicular networks nodes [17], and supports data dissemination

The associate editor coordinating the review of this manuscript and approving it for publication was Fuhui Zhou.

through cluster head nodes to reduce the complexity of end-to-end communication [18], [19]. This clustering method has been widely employed in V2X communications to improve the performance of vehicular network [20]–[24]. The authors in [20] utilized a clustering method for predicting the movement of vehicle groups to increase the connection probability of V2V communications. Although the node with the largest link duration is selected as the cluster head in this method, the stability of the vehicle cluster may still not be maintained due to dynamic road traffic. In [21], a stable clustering method based on vehicular multi-hop communication was proposed, which adopts the relative mobility metric between vehicles to select out the cluster-head vehicles (CHVs). However, in order to increase the packet transmission rate among vehicles, this method causes a certain degree of propagation delay. For improving the end-to-end latency for vehicular network topology, a cluster-based protocol for selecting the optimal intersection CHV on the basis of real-time traffic was proposed in [22]. However, this protocol causes too much overhead for the vehicle cluster. In [23], an evolutionary game method for optimizing vehicle clustering was proposed to reduce the overhead of cluster recombination in vehicular networks. Although the method can automatically classify the vehicles and pick out CHVs, it just considers the average speed of vehicles rather than the dynamic speed of each vehicle. In [24], a dynamic clustering algorithm for considering real-time speed and position of vehicles was proposed. However, this algorithm needs as input the length of the cluster in order to create the vehicles clustering. In fact, pre-estimating the length of different vehicle clusters for dynamic road traffic is complicated as well as inconvenient. In this paper, we propose a clustering method that not only dynamically classifies vehicles but also adjusts cluster size according to real-time road traffic. Furthermore, the selected CHVs by this method can achieve an optimal trade-off between the CHVs' relative speed and power allocation.

The expansion of vehicular networks has resulted in a tremendous increase in energy consumption, and power control is an effective way to reduce the power consumption without degrading both the connectivity and the coverage of vehicular networks [25], [26]. To balance the power allocation among CHVs to further increase the downlink throughput, the power control method is applied in V2X communications. As described above, NOMA has developed power-domain multiplexing to meet the requirements of high overload transmission [12]. Motivated by this, some researchers have studied power control schemes in V2X communications based on NOMA [13], [27]–[29]. In [27], a NOMA-based power allocation algorithm with opportunistic constraints is proposed to increase the throughput of V2X communications. For pursuing the robustness in vehicular communication, the algorithm only relies on the distance between the BS and vehicles to allocate the transmission power, thereby ignoring the dynamic power allocation issues of vehicles switching between different base stations. In [28], a NOMA-enabled hierarchical power control method was proposed for dynamically power allocation from BSs to vehicles which optimizes the energy efficiency of the vehicular networks. Although this method exhibits excellent performance in terms of switching rate as well as spectrum efficiency, it inevitably has a certain degree of feedback delay. In order to avoid the access delay and matching instability caused by the mobility of vehicles, a hybrid power control scheme based on NOMA was proposed in [13]. This scheme autonomously allocates power-domain resources in a centralized and distributed manner through the BS and vehicles, respectively. Nevertheless, its multiplexing performance is inferior to the power control approach mentioned in [29]. The approach in [29] took full advantage of the cooperative performance of multiple-input multiple-output (MIMO) and NOMA, which maximizes bandwidth efficiency by multi-antenna spatial diversity and power-domain multiplexing. In recent years, NOMA-based cooperative transmission has been considered as a virtual MIMO scheme that can improve bandwidth efficiency of the system and reliability of users communication [30], [31]. In [32], a NOMA-based cooperative method is utilized to improve the performance of V2X communications with an emphasis on enhancing the throughput of remote transmission links. However, the corresponding throughput to the farthest transmission link is not always the smallest since the user in this link is assigned a maximum power allocation. Therefore, we propose a power control strategy based on NOMA cooperative transmission to maximize the achievable rates of CHVs, where the proposed power control strategy not only improves the throughput of the vehicular networks but also balances the power allocation among CHVs.

The rest of this paper is organized as follows. Section II describes the system model. Section III proposes a clustering algorithm and power allocation strategy. Section IV provides numerical simulation results and discussions. Finally, Section V concludes this paper.

II. SYSTEM MODEL

Car-following model is a microscopic traffic flow model in which vehicles are traveling on a single line [33], [34]. Vehicles on the road have a certain degree of interaction due to their own mobility [21], thus the car-following model can capture the driving state of vehicles by variables such as speed and position [35]–[37]. Focusing on the impact of real-time traffic and road conditions for V2X communication system, a clustering car-following model is shown in Fig. 1, where each cluster includes the vehicles in green ellipsis area, and the CHVs are marked with a star symbol. The BS firstly uses a NOMA technique to send messages to the CHVs, and then the CHVs utilize a cooperative method to share inter-cluster information. Finally, other vehicles in each cluster only need to receive the broadcast messages from their CHVs. On the one hand, the hierarchical topology structure in vehicular network is established by the clustering method. On the other hand, the CHV acts as a local controller to support data dissemination between cluster members and clusters,

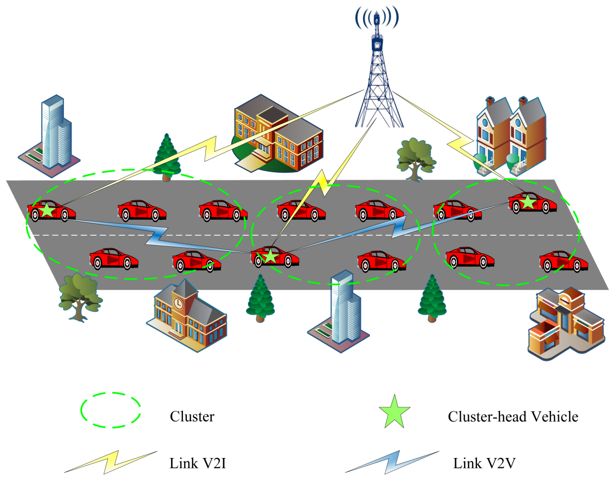

FIGURE 1. A clustering car-following model for V2X communications system.

which reduces the complexity of end-to-end communication in vehicular network. Therefore, the communication complexity of vehicular network topology can be reduced.

A downlink transmission scenario which contains a BS and three CHVs to preform NOMA is shown in Fig. 2. According to the near-far effect, the power-domain NOMA allocates less power resources to users with good channel gains. The tri-user mode not only representatively presents the power domain differences between users, but also facilitates the analysis and deployment of cooperative NOMA. Therefore, three CHVs' power allocation are enough to demonstrate the key aspects of power allocation among vehicles while avoiding unnecessary complications. Note that although we limit ourselves to three CHVs, the proposed approach can be extended to multiple CHVs. In Fig. 2, the BS and CHV-3 are regarded as the "source" node and the destination node; CHV-1 and CHV-2 are considered as the destination nodes or the relay nodes, respectively. The distance between the BS and the three CHVs satisfies $d_{B1} < d_{B2} < d_{B3}$, We assume

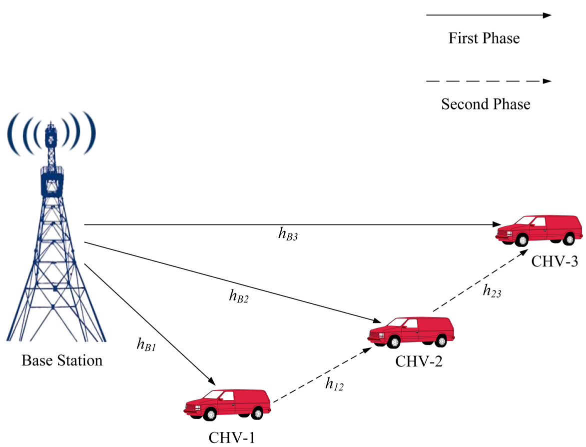

FIGURE 2. Tri-CHV NOMA cooperative model.

that the BS sends the message to three CHVs with a total transmission power P_B, and each CHV is equipped with an antenna and it operates in half-duplex mode. We divide the message transmission process into two phases. The first phase is the transmission of V2I links, where the BS sends the total superposition message to three CHVs, respectively. The second phase is the transmission of V2V links (i.e., links CHV-1→CHV-2 and CHV-2→CHV-3), where the amplify-and-forward (AF) protocol is employed by CHV-1 and CHV-2. For V2I communications where only the receivers are in motion, some theoretical analysis and experimental results demonstrate that the received signal amplitude of V2I links may follow the Rayleigh distribution [38], [39]. Note that the propagation channels of V2V communications are more dynamic than those in V2I, thus the envelope of the resulting narrowband impulse response should be modeled using the dual-Rayleigh distribution [40], [41]. Therefore, the channels of V2I communication scenarios can be modeled as Rayleigh fading, while the channels of V2V communication scenarios are modeled as dual-Rayleigh fading.

The total message sent by BS to the three NOMA-based CHVs is denoted as

$$x = \sqrt{P_B} \cdot \sum\nolimits_{i=1}^{3} a_i x_i, \tag{1}$$

where a_i^2 $(i = 1, 2, 3)$ is the power allocation coefficient, x_1, x_2 and x_3 are the messages that satisfy $E\left[|x_i|^2\right] = 1$. According to the channel qualities, we assume $0 < a_1^2 < a_2^2 < a_3^2$ and $a_1^2 + a_2^2 + a_3^2 \leq 1$. In the first phase, the signals received by CHV-1, CHV-2 and CHV-3 are respectively given by

$$y_{B\to 1}^1 = xh_{B1} + n_1, \tag{2}$$
$$y_{B\to 2}^1 = xh_{B2} + n_2, \tag{3}$$
$$y_{B\to 3}^1 = xh_{B3} + n_3, \tag{4}$$

where h_{Bi} is the Rayleigh channel fading coefficient from BS to CHV, and follows the complex Gaussian distribution with the mean of zero and the variance of Ω_{Bi}, i.e., $h_{Bi} \sim CN(0, \Omega_{Bi})$. We assume that all channels are only affected by additive white Gaussian noise (AWGN), n_1, n_2 and n_3 are the AWGN with variance of N_0 at CHV-1, CHV-2 and CHV-3, respectively.

To ensure that the received signals are successfully decoded and that there is successive interference cancellation (SIC) at CHVs [42], [43], we consider that the predefined target transmission rates of link BS CHV is lower than the corresponding achievable rates. In the case, for the transmission link BS CHV-1, we have

$$\begin{cases} R_{B\to 1}^{x_3} \leq \log_2\left(1 + \gamma_{B\to 1}^{x_3}\right) \\ R_{B\to 1}^{x_2} \leq \log_2\left(1 + \gamma_{B\to 1}^{x_2}\right), \end{cases} \tag{5}$$

where $R_{B\to 1}^{x_3}$ and $R_{B\to 1}^{x_2}$ are the predefined target data rates of the messages x_3 and x_2 at CHV-1, respectively. The SINR for decoding the messages x_3 and x_2 at CHV-1 are respectively denoted as

$$\gamma_{B\to 1}^{x_3} = \frac{\frac{P_B}{N_0}a_3^2|h_{B1}|^2}{\frac{P_B}{N_0}\left(a_1^2+a_2^2\right)|h_{B1}|^2+1}, \tag{6}$$

$$\gamma_{B\to 1}^{x_2} = \frac{\frac{P_B}{N_0}a_2^2|h_{B1}|^2}{\frac{P_B}{N_0}a_1^2|h_{B1}|^2+1}. \tag{7}$$

Therefore, the achievable data rates of the message x_1 for the transmission link BS→CHV-1 is given by

$$C_{B\to 1}^{x_1} = \log_2\left(1+\gamma_{B\to 1}^{x_1}\right), \tag{8}$$

where $\gamma_{B\to 1}^{x_1}$ is the SINR for decoding the message x_1 at CHV-1,

$$\gamma_{B\to 1}^{x_1} = \frac{P_B a_1^2|h_{B1}|^2}{N_0}. \tag{9}$$

In order to realize SIC for the transmission link BS→CHV-2, we have

$$R_{B\to 2}^{x_3} \leq \log_2\left(1+\gamma_{B\to 2}^{x_3}\right), \tag{10}$$

where $R_{B\to 2}^{x_3}$ is the predefined target data rates of the message x_1 at CHV-2, and $\gamma_{B\to 2}^{x_3}$ is the SINR for decoding the message x_3 at CHV-2,

$$\gamma_{B\to 2}^{x_3} = \frac{\frac{P_B}{N_0}a_3^2|h_{B2}|^2}{\frac{P_B}{N_0}\left(a_1^2+a_2^2\right)|h_{B2}|^2+1}. \tag{11}$$

After the message x_3 are successfully decoded at CHV-2, the SINR for decoding the message x_2 at CHV-2 is given by

$$\gamma_{B\to 2}^{x_2} = \frac{\frac{P_B}{N_0}a_2^2|h_{B2}|^2}{\frac{P_B}{N_0}a_1^2|h_{B2}|^2+1}, \tag{12}$$

and the achievable data rates of the message x_2 for the transmission link BS→CHV-2 is given by

$$C_{B\to 2}^{x_2} = \log_2\left(1+\gamma_{B\to 2}^{x_2}\right). \tag{13}$$

Since the signal power of the message x_3 is stronger than messages x_2 and x_1, the SINR for decoding the message x_3 at CHV-3 is directly given by

$$\gamma_{B\to 3}^{x_3} = \frac{\frac{P_B}{N_0}a_3^2|h_{B3}|^2}{\frac{P_B}{N_0}\left(a_1^2+a_2^2\right)|h_{B3}|^2+1}, \tag{14}$$

and the achievable data rates for the transmission link BS CHV-3 is expressed as

$$C_{B\to 3}^{x_3} = \log_2\left(1+\gamma_{B\to 3}^{x_3}\right). \tag{15}$$

To ensure that the signals received by CHVs are successfully decoded in the first phase, we have

$$\begin{cases} R_{B\to 1}^{x_3} \leq \log_2\left(1+\gamma_{B\to 1}^{x_3}\right) \\ R_{B\to 1}^{x_2} \leq \log_2\left(1+\gamma_{B\to 1}^{x_2}\right) \\ R_{B\to 2}^{x_3} \leq \log_2\left(1+\gamma_{B\to 2}^{x_3}\right). \end{cases} \tag{16}$$

Under the constraints of predefined target rates and $a_1^2+a_2^2+a_3^2 \leq 1$, the power allocation coefficients are described as follows,

$$a_1^2 \in \left(0, \frac{\gamma|h_{B1}|^2 - R_1 - R_2(1+R_1)}{\gamma|h_{B1}|^2(1+R_1)(1+R_2)}\right], \tag{17}$$

$$a_2^2 \in \left(0, \frac{\gamma|h_{B1}|^2 R_2 + R_2}{\gamma|h_{B1}|^2(1+R_1)(1+R_2)}\right], \tag{18}$$

$$a_3^2 \in \left(0, \frac{R_3|h_{B2}|^2\left(\gamma|h_{B1}|^2-R_1\right)}{\gamma|h_{B1}|^2|h_{B2}|^2(1+R_1)} + \frac{R_3|h_{B1}|^2(1+R_1)}{\gamma|h_{B1}|^2|h_{B2}|^2(1+R_1)}\right], \tag{19}$$

where $\gamma = \frac{P_B}{N_0}$, $R_1 = 2^{R_{B\to 1}^{x_3}}-1$, $R_1 = 2^{R_{B\to 1}^{x_2}}-1$ and $R_1 = 2^{R_{B\to 2}^{x_3}}-1$.

In the second phase (i.e., cooperative phase), CHV-1 transmits the decoded message $y_{B\to 1}^1$ to CHV-2, while CHV-2 transmits the decoded message $y_{B\to 2}^1$ to CHV-3. The cooperative transmission links CHV-1→CHV-2 and CHV-2→CHV-3 choose AF to forward the information. The corresponding amplify factors of links CHV-1→CHV-2 and CHV-2→CHV-3 are respectively given by [44]

$$\alpha = \sqrt{\frac{P_{V1}}{P_B|h_{B1}|^2+N_0}}, \tag{20}$$

$$\beta = \sqrt{\frac{P_{V2}}{P_B|h_{B2}|^2+N_0}}, \tag{21}$$

where P_{V1} and P_{V2} are the transmission power of CHV-2 and CHV-3, respectively. Therefore, the received signals by CHV-2 and CHV-3 can be expressed as

$$y_{1\to 2}^2 = \alpha y_{B\to 1}^1 h_{12} + n_{12}, \tag{22}$$

$$y_{2\to 3}^2 = \beta y_{B\to 2}^1 h_{23} + n_{23}. \tag{23}$$

The channels of links CHV-1→CHV-2 and CHV-2→CHV-3 are modeled as dual-Rayleigh fading, h_{12} and h_{23} are the products of two i.i.d (independent and identically distributed) complex Gaussian random variables [45], i.e., $h_{12} = h_{12}^x h_{12}^y$ and $h_{23} = h_{23}^x h_{23}^y$, where each of the random variable has zero mean and variance of Ω_v per dimension. We make the following two realistic assumptions.

Case I: If a_3^2 meets the following conditions

$$a_3^2 \in \left(0, \frac{R_4\gamma|h_{B1}|^2\gamma_1|h_{12}|^2}{\gamma|h_{B1}|^2\gamma_1|h_{12}|^2(1+R_4)} + \frac{R_4\left(\gamma|h_{B1}|^2+\gamma_1|h_{12}|^2+1\right)}{\gamma|h_{B1}|^2\gamma_1|h_{12}|^2(1+R_4)}\right], \tag{24}$$

where we utilize $Z = 0$ to describe the Case I. For the cooperative link CHV-1→CHV-2, the message x_2 failed to be decoded at CHV-2. In Case I, the information received at

CHV-2 does not obtain the cooperative gain, and the achievable data rates at CHV-2 is given by

$$C_2^{Z=0} = \log_2\left(1+\gamma_{B\to 2}^{x_2}\right). \tag{25}$$

Case II: If a_3^2 meets the following conditions

$$\begin{aligned} a_3^2 \in & \left(\frac{R_4\gamma|h_{B1}|^2\gamma_1|h_{12}|^2}{\gamma|h_{B1}|^2\gamma_1|h_{12}|^2(1+R_4)}\right. \\ & + \frac{R_4\gamma|h_{B1}|^2\gamma_1|h_{12}|^2}{\gamma|h_{B1}|^2\gamma_1|h_{12}|^2(1+R_4)}, \frac{R_3|h_{B2}|^2\left(\gamma|h_{B1}|^2-R_1\right)}{\gamma|h_{B1}|^2|h_{B2}|^2(1+R_1)} \\ & \left. + \frac{R_3|h_{B1}|^2(1+R_1)}{\gamma|h_{B1}|^2|h_{B2}|^2(1+R_1)}\right], \end{aligned} \tag{26}$$

where $\gamma_1 = \frac{P_{V1}}{N_0}$, $R_4 = 2^{R_{1\to 2}^{x_3}} - 1$. We use $Z = 1$ to depict the case II. At CHV-2, SIC will be realized for the cooperative link CHV-1→CHV-2, i.e.,

$$R_{1\to 2}^{x_3} \le \log_2\left(1+\gamma_{1\to 2}^{x_3}\right), \tag{27}$$

where $R_{1\to 2}^{x_3}$ is the predefined target data rates of cooperative link CHV-1→CHV-2 with respect to the message x_3, and the corresponding SINR $\gamma_{1\to 2}^{x_3}$ for decoding the message x_3 at CHV-2 is given by (28), as shown at the bottom of this page. After the message x_3 are successfully decoded at CHV-2, the SINR for decoding the message x_2 at CHV-2 can be expressed as

$$\gamma_{1\to 2}^{x_2} = \frac{\frac{P_B}{N_0}a_2^2|h_{B1}|^2\frac{P_{V1}}{N_0}|h_{12}|^2}{\frac{P_B}{N_0}a_1^2|h_{B1}|^2\frac{P_{V1}}{N_0}|h_{12}|^2+\frac{P_B}{N_0}|h_{B1}|^2+\frac{P_{V1}}{N_0}|h_{12}|^2+1}, \tag{29}$$

and thus the achievable data rates at CHV-2 in Case II is denoted as

$$C_2^{Z=1} = \log_2\left(1+\gamma_{B\to 2}^{x_2}+\gamma_{1\to 2}^{x_2}\right). \tag{30}$$

As for the cooperative transmission link CHV-2 CHV-3, the SINR for decoding the message x_3 at CHV-3 is given by (31), as shown at the bottom of this page.

At the end of the second phase, maximum-ratio combining (MRC) [46], [47] is performed to detect the messages for CHV-2 and CHV-3. Consequently, the achievable data rates at CHV-1, CHV-2 and CHV-3 are respectively expressed as

$$C_1 = \frac{1}{2}\log_2\left(1+\gamma_{B\to 1}^{x_1}\right), \tag{32}$$

$$C_2 = \left[\frac{1}{2}\log_2\left(1+\gamma_{B\to 2}^{x_2}\right)\right]^{1-Z} \times \left[\frac{1}{2}\log_2\left(1+\gamma_{B\to 2}^{x_2}+\gamma_{1\to 2}^{x_2}\right)\right]^{Z}, \tag{33}$$

$$C_3 = \frac{1}{2}\log_2\left(1+\gamma_{B\to 3}^{x_3}+\gamma_{2\to 3}^{x_3}\right). \tag{34}$$

III. CLUSTERING ALGORITHM AND POWER ALLOCATION

A. VEHICLES CLUSTERING

There is a certain interaction between the vehicles on the road, and the car-following model as a microscopic traffic flow model can reflect the driving state of the vehicles on the road by speed and position. In this subsection, we can take the change of real-time traffic condition into account in the process of vehicles clustering, making the clustering algorithm more suitable for actual traffic scenarios. We firstly utilize the car-following distance to cluster the vehicles and adjust the cluster size according to the vehicle's relative speed and delay interval on the road. And then, joint vehicle relative speed and transmission power of vehicles are employed to select out CHVs.

We suppose that there are n $(k = 1, 2, \cdots, n)$ vehicles near a BS in a single lane. The criterion for vehicles clustering is that the distance between the two adjacent cars is not farther than the minimum safety distance, and the coverage of the vehicle cluster is within the communication radius. According to the difference of the car-following distances between adjacent vehicles and the sum of the car-following distances in each cluster, we have

$$\begin{cases} |S_{k+1}-S_k| \le d_{\min} \\ \sum_{k=1}^{w-1} S_k < D, \end{cases} \tag{35}$$

where w $(j = 1, 2, \cdots, w)$ is the number of vehicles contained in a cluster, $d_{\min}$ represents the minimum safe distance between the adjacent vehicles, D denotes the communication radius, and the car-following distance S_k is expressed as

$$S_k = d_{\min} + \Delta v \cdot \tau. \tag{36}$$

where τ in formula (36) is the delay interval, and Δv represents the relative speed difference between adjacent vehicles, i.e.,

$$\Delta v = |v_k - v_{k-1}|, \tag{37}$$

where v_k denotes the speed of vehicle k.

After the vehicles on the road are clustered, we next proceed with the selection of CHVs. It is known that the transmission power assigned to each vehicle by BS is different, and there is also a difference in the speed of each vehicle within a cluster. Taking into account the above issues, in order to

$$\gamma_{1\to 2}^{x_3} = \frac{\frac{P_B}{N_0}a_3^2|h_{B1}|^2\frac{P_{V1}}{N_0}|h_{12}|^2}{\frac{P_B}{N_0}\left(a_1^2+a_2^2\right)|h_{B1}|^2\frac{P_{V1}}{N_0}|h_{12}|^2+\frac{P_B}{N_0}|h_{B1}|^2+\frac{P_{V1}}{N_0}|h_{12}|^2+1} \tag{28}$$

$$\gamma_{2\to 3}^{x_3} = \frac{\frac{P_B}{N_0}a_3^2|h_{B2}|^2\frac{P_{V2}}{N_0}|h_{23}|^2}{\frac{P_B}{N_0}\left(a_1^2+a_2^2\right)|h_{B2}|^2\frac{P_{V2}}{N_0}|h_{23}|^2+\frac{P_B}{N_0}|h_{B2}|^2+\frac{P_{V2}}{N_0}|h_{23}|^2+1} \tag{31}$$

select the vehicle with the lower relative speed and optimal transmission power as the CHV, we define the CHV selection parameter as

$$M_c = \max_c \left[p_c \cdot \frac{P_V}{(w-1)} \cdot \sum_{j=1,c\neq j}^{w-1} |\bar{h}_{cj}|^2 \cdot (\bar{S}_{cj})^{-\alpha} \right], \quad (38)$$

where P_v is the transmission power of vehicle, α is the path loss factor, $\bar{h}_{cj}$ is the average channel gain between the CHV and its member vehicles, which follows dual-Rayleigh fading with zero mean and variance of Ω_{cj} per dimension. We define $p_c = P_c/P_T$, P_C is the transmission power required by BS to transmit the message to a certain vehicle in one cluster and P_T is the total transmit power of BS to send a message to all the vehicles inside the cluster. Here, $\bar{S}_{cj}$ denotes the average normalized car-following distance between the CHV and its member vehicles,

$$\bar{S}_{cj} = \frac{d_{\min} + \Delta v_{cj} \cdot \bar{\tau}_{cj}}{\sum_{j=1,c\neq j}^{w-1} S_j}, \quad (39)$$

where S_j is the car-following distance among the member vehicles, $\bar{\tau}_{cj}$ is the mean of the delay interval between the CHV and its member vehicles. The relative speed Δv_{cj} of CHV is given by

$$\Delta v_{cj} = \sqrt{\frac{1}{w-1} \sum_{j=1,c\neq j}^{w-1} \left(v_c - \frac{1}{w} \sum_{j=1}^{w} v_j \right)^2}, \quad (40)$$

where Δv_{cj} is obtained by calculating the standard deviation of the average speed between each vehicle and all the vehicles in the cluster. v_c and v_j represent the speeds of the CHV and the member vehicle, respectively.

B. POWER ALLOCATION

Although we have already considered the transmission power ratio p_c as one of the significant factors affecting the selection of the CHV, there may be still a few CHVs with poor quality communication links due to being far away from the BS. We next propose an interval-based optimal power control scheme to maximize the achievable rates of CHVs while BS transmission power is limited, thereby improving the throughput of the vehicular network and balancing the power allocation among CHVs.

To simplify the analysis for the V2V communication process, we assume that CHVs have the same transmission power P_V, i.e., $P_{V1} = P_{V2} = P_V$. In this case, the optimal power allocation problem (i.e., maximizing the minimum achievable rate of CHV at the limited transmission power of BS) can be given by

$$\begin{cases} \max\limits_{P_i} \min \left[C_1(P_i), C_2(P_i), C_3(P_i) \right] \\ \text{s.t. } P_1 + P_2 + P_3 \leq P_B \\ \quad P_i \geq 0, i = 1, 2, 3, \end{cases} \quad (41)$$

where $P_1 = a_1^2 P_B$, $P_2 = a_2^2 P_B$ and $P_3 = a_3^2 P_B$. We define $P_B = P_i/a_i^2$, then optimization problem (41) can be converted into the following problem

$$\begin{cases} \max\limits_{a_i^2} \min \left[C_1(a_i^2), C_2(a_i^2), C_3(a_i^2) \right] \\ \text{s.t. } a_1^2 + a_2^2 + a_3^2 \leq 1 \\ \quad a_i^2 \geq 0, i = 1, 2, 3. \end{cases} \quad (42)$$

where a_i^2 denotes the power allocation coefficient. Since the optimization problem formulated in (42) is non-convex, it's hard to directly obtain the solution. Therefore, we turn it into a series of linear optimization problems and adopt an interval-based dichotomy to solve them.

If the objective function is a quasi-concave function, the optimization problem is quasi-concave when its constraints are convex. The objective function in (42) is non-convex and its constraints are linear, which implies that the optimization problem is quasi-concave. As such, all the subsets of the objective function are concave. Here, we denote the subset of the objective function as [48]

$$\mathbb{C}_\theta = \left\{ \min\left[C_1\left(a_i^2\right), C_2\left(a_i^2\right), C_3\left(a_i^2\right) \right] \geq \theta, \theta \in \mathbb{R} \right\}, \quad (43)$$

and the constraints of $\mathbb{C}$ can be expressed as

$$\begin{cases} a_1^2 \dfrac{P_B|h_{B1}|^2}{N_0} \geq 2^{2\theta} - 1 \\ a_2^2 \dfrac{P_B|h_{B2}|^2}{a_1^2 P_B|h_{B2}|^2 + N_0} \geq 2^{2\theta} - 1, (Z=0) \\ a_2^2 \left(\dfrac{P_B|h_{B1}|^2 \frac{P_V}{N_0}|h_{12}|^2}{a_1^2 P_B|h_{B1}|^2 N_0 \frac{P_V}{N_0}|h_{12}|^2 + P_B|h_{B1}|^2 + P_V|h_{12}|^2 + N_0} + \dfrac{P_B|h_{B2}|^2}{a_1^2 P_B|h_{B2}|^2 + N_0} \right) \geq 2^{2\theta} - 1, (Z=1) \\ a_3^2 \left[\dfrac{P_B|h_{B2}|^2 \frac{P_V}{N_0}|h_{23}|^2}{\left(a_1^2 + a_2^2\right) P_B|h_{B2}|^2 \frac{P_V}{N_0}|h_{23}|^2 + P_B|h_{B2}|^2 + P_V|h_{23}|^2 + N_0} + \dfrac{P_B|h_{B3}|^2}{\left(a_1^2 + a_2^2\right) P_B|h_{B3}|^2 + N_0} \right] \geq 2^{2\theta} - 1, \end{cases} \quad (44)$$

Obviously, the inequalities in (44) are linear.

Here, we suppose $\hat{\psi}$ is the optimal max-min value of (42). Finding the optimal value of a_i^2 that satisfies the following conditions for a constant value θ ($\theta \geq 0$),

$$\begin{cases} C_i \geq \theta \\ a_1^2 + a_2^2 + a_3^2 \leq 1 \\ a_i^2 > 0 \end{cases}, \quad (45)$$

where C_i is the minimum achievable rate of CHVs. If the conditions (45) are feasible then we get $\hat{\psi} \geq \theta$, otherwise we consider that $\hat{\psi} \leq \theta$. Equivalently, (45) can be re-formulated as

$$\begin{cases} \min a_1^2 + a_2^2 + a_3^2 \\ s.t.\ C_i \geq \theta, i = 1, 2, 3 \\ \quad a_i^2 > 0. \end{cases} \tag{46}$$

In order to obtain the closed-form optimal solution of formula (46), we use the following proposition.

Proposition 1: For a constant value θ, the optimization solution of formula (46) is given by

$$a_1^2 = \frac{\left(2^{2\theta} - 1\right) N_0}{P_B |h_{B1}|^2}, \tag{47}$$

$$a_2^2 = \left[\frac{\left(2^{2\theta} - 1\right) |h_{B2}|^2 + |h_{B1}|^2}{P_B |h_{B1}|^2 |h_{B2}|^2} \cdot \left(2^{2\theta} - 1\right) N_0\right]^{1-Z} \times \left(\frac{2^{2\theta} - 1}{c + d}\right)^Z, \tag{48}$$

$$a_3^2 = \left(\frac{2^{2\theta} - 1}{m + n}\right)^{1-Z} \cdot \left(\frac{2^{2\theta} - 1}{p + q}\right)^Z, \tag{49}$$

where

$$c = \frac{P_B |h_{B1}|^2 |h_{B2}|^2}{\left(2^{2\theta} - 1\right) |h_{B2}|^2 N_0 + |h_{B1}|^2 N_0}, \tag{50}$$

$$d = \frac{P_B |h_{B1}|^2 P_V |h_{12}|^2}{\left(2^{2\theta} - 1\right) P_V |h_{12}|^2 + P_B |h_{B1}|^2 + P_V |h_{12}|^2 + N_0} \times \frac{1}{N_0}, \tag{51}$$

$$e = \frac{\left(2^{2\theta} - 1\right) N_0}{P_B |h_{B1}|^2} \cdot \left(2^{2\theta} + \frac{|h_{B1}|^2}{|h_{B2}|^2}\right), \tag{52}$$

$$f = \frac{\left(2^{2\theta} - 1\right) N_0}{P_B |h_{B1}|^2} + \frac{2^{2\theta} - 1}{c + d}, \tag{53}$$

$$m = \frac{P_B |h_{B3}|^2}{e \cdot P_B |h_{B3}|^2 + N_0}, \tag{54}$$

$$n = \frac{P_B |h_{B2}|^2 \cdot \frac{P_V}{N_0} |h_{23}|^2}{e \cdot P_B |h_{B2}|^2 \cdot \frac{P_V}{N_0} |h_{23}|^2 + P_B |h_{B2}|^2 + P_V |h_{23}|^2 + N_0}, \tag{55}$$

$$p = \frac{P_B |h_{B3}|^2}{f \cdot P_B |h_{B3}|^2 + N_0}, \tag{56}$$

$$q = \frac{P_B |h_{B2}|^2 \cdot \frac{P_V}{N_0} |h_{23}|^2}{f \cdot P_B |h_{B2}|^2 \cdot \frac{P_V}{N_0} |h_{23}|^2 + P_B |h_{B2}|^2 + P_V |h_{23}|^2 + N_0}. \tag{57}$$

Proof: See Appendix.

To ensure the optimal values of satisfying conditions (17), (18), (19) and $\sum_i^3 a_i^2 \leq 1$, we design an interval-based optimal power control scheme as described in Algorithm 1. Here, ψ_L and ψ_U are the lower and upper limits of the initialized $\mathbb{C}_\theta$, $\hat{a}_i^2$ represents the optimal value of a_i^2, δ is a minimum value and denotes the accuracy range.

Algorithm 1 Interval-Based Optimal Power Control Scheme

Input: $\psi_L, \psi_U, \delta, Z, i = 1, 2, 3$;
While $\psi_U - \psi_L \geq \delta$ **do**
  Set $\theta = \frac{\psi_U + \psi_L}{2}$;
  Switch (Z)
    Case I: Set $Z = 0$ and solve the convex problem of formula (46) to obtain the optimal a_i^2;
      if $a_3^2 > \frac{R_4 \gamma |h_{B1}|^2 \gamma_1 |h_{12}|^2 + R_4 (\gamma |h_{B1}|^2 + \gamma_1 |h_{12}|^2 + 1)}{\gamma |h_{B1}|^2 \gamma_1 |h_{12}|^2 (1 + R_4)}$
      then
      $\widehat{a}_3^2 = \frac{R_4 \gamma |h_{B1}|^2 \gamma_1 |h_{12}|^2 + R_4 (\gamma |h_{B1}|^2 + \gamma_1 |h_{12}|^2 + 1)}{\gamma |h_{B1}|^2 \gamma_1 |h_{12}|^2 (1 + R_4)}$
      else $\widehat{a}_3^2 = a_3^2$
      end if
    break
    Case II: Set $Z = 1$ and solve the convex problem of formula (46) to obtain the optimal a_i^2;
      if $a_3^2 > \frac{R_3 |h_{B2}|^2 (\gamma |h_{B1}|^2 - R_1) + R_3 |h_{B1}|^2 (1 + R_1)}{\gamma |h_{B1}|^2 |h_{B2}|^2 (1 + R_1)}$
      then
      $\widehat{a}_3^2 = \frac{R_3 |h_{B2}|^2 (\gamma |h_{B1}|^2 - R_1) + R_3 |h_{B1}|^2 (1 + R_1)}{\gamma |h_{B1}|^2 |h_{B2}|^2 (1 + R_1)}$
      else $\widehat{a}_3^2 = a_3^2$
      end if
    break
  if $a_1^2 + a_2^2 + \widehat{a}_3^2 \leq 1$ **then**
    Set $\psi_L = \theta, \widehat{a}_1^2 = a_1^2, \widehat{a}_2^2 = a_2^2, \hat{a}_3^2 = \widehat{a}_3^2, \hat{\psi} = \theta$;
  else $\psi_u = \theta$
  end if
end while
if $\widehat{a}_2^2 > \frac{\gamma |h_{B1}|^2 R_2 + R_2}{\gamma |h_{B1}|^2 (1 + R_1)(1 + R_2)}$ **then**
  $\hat{a}_2^2 = \frac{\gamma |h_{B1}|^2 R_2 + R_2}{\gamma |h_{B1}|^2 (1 + R_1)(1 + R_2)}$
else $\hat{a}_2^2 = \widehat{a}_2^2$
end if
if $\widehat{a}_1^2 > \frac{\gamma |h_{B1}|^2 - R_1 - R_2 (1 + R_1)}{\gamma |h_{B1}|^2 (1 + R_1)(1 + R_2)}$ **then**
  $\hat{a}_1^2 = \frac{\gamma |h_{B1}|^2 - R_1 - R_2 (1 + R_1)}{\gamma |h_{B1}|^2 (1 + R_1)(1 + R_2)}$
else $\hat{a}_1^2 = \widehat{a}_1^2$
end if
Output: $\hat{a}_1^2, \hat{a}_2^2, \hat{a}_3^2$.

IV. NUMERICAL SIMULATION RESULTS

In this section, numerical simulation results are provided for evaluating the performance of the clustering algorithm and the proposed power allocation scheme. These results are compared with the conventional NOMA [31] as well as the fixed NOMA [49] algorithms.V2I and V2V transmission links are modeled as Rayleigh fading channel and dual-Rayleigh fading channel, respectively.

Fig. 3 shows the three-dimensional relationship among the size of vehicle cluster, the inter-vehicle speed difference and

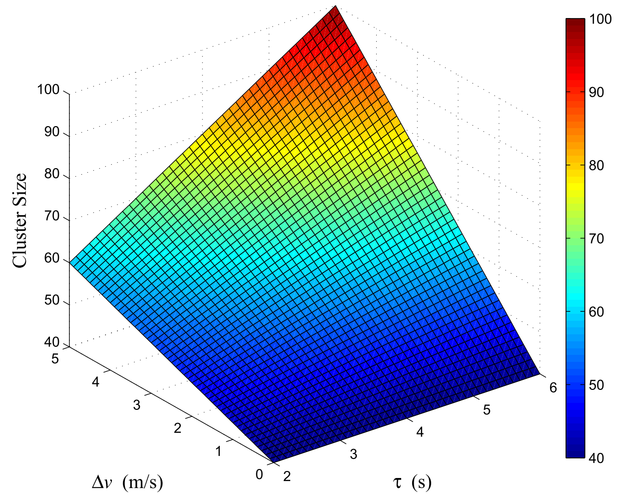

FIGURE 3. The cluster size versus inter-vehicle speed difference (Δv) and delay interval (τ).

delay interval. Here, we set $d_{\min} = 20$ m and $D = 100$ m. It is obvious that the coverage of vehicle cluster gradually expands as blue color turns red when the inter-vehicle speed difference and the delay interval are increasing, which implies that the algorithm dynamically adjusts the cluster size according to the actual traffic and road conditions. Moreover, it can be seen that the vehicle cluster size is maintained in the range of approximately 40-100 meters due to the limitation of the following distance between adjacent vehicles. Therefore, the adverse impact of the excessive size of cluster on communication quality of V2V links is reduced.

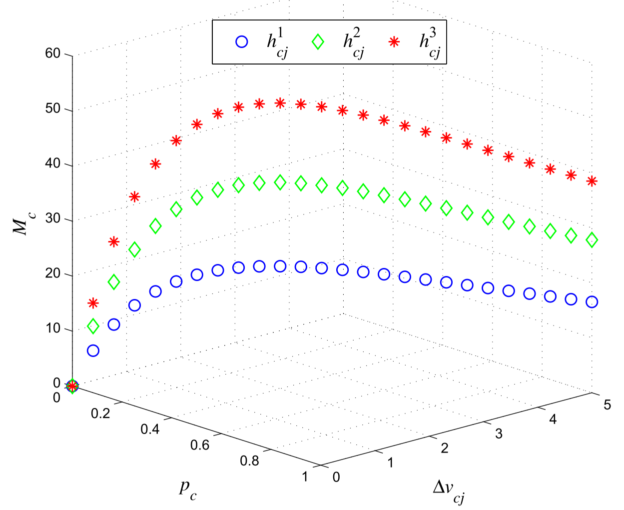

FIGURE 4. CHV selection parameter versus inter-vehicle speed difference (Δv_{cj}) and transmission power ratio (p_c) under different channel gains ($\bar{h}_{cj}$).

Fig. 4 plots the relationship among CHV selection parameter, inter-vehicle speed difference and transmission power ratio under different channel gain conditions. Here, we set the parameters as $\bar{\tau}_{cj} = 5$ and $P_V = 27$ dBm. The cluster size is set equal to 100 meters and the path loss factor is set as $\alpha = 3$ [50]. The blue, green and red color curves correspond to different dual-Rayleigh fading channels coefficient $\bar{h}_{cj}$ with per dimension variance $\Omega^1_{cj} = 3$, $\Omega^2_{cj} = 5$ and $\Omega^3_{cj} = 7$, respectively. As we can be seen from Fig. 4, the CHV selection parameters of the blue curve are always larger than those of green and red under the same conditions of Δv_{cj} and p_c, i.e., the vehicle with bigger channel gain is easily selected as CHV. Furthermore, we can observe that M_c increases first and then decreases with the increase of Δv_{cj} and p_c. The corresponding extreme points of M_c are obtained when $\Delta v_{cj} = 2$ and $p_c = 0.4$, which is favorable for selecting the CHV which can balance Δv_{cj} and p_c to maintain cluster stability and reduce overhead. As expected, the numerical simulation results are consistent with the analysis values.

As shown below in Fig. 5 to Fig. 9, we investigate the convergence of proposed power control algorithm and minimum achievable rate of CHV in two cases (Case I and Case II), respectively. We set some parameters as follows: $\delta = 10^{-5}$, $\psi_L = 0$ bit/s/Hz, $N_0 = 1$, $\psi_u = 1$ bit/s/Hz, $P_B = 30$ dBm, $P_V = 27$ dBm, $\Omega_{B1} = 1$, $\Omega_{B2} = 8$ and $\Omega_{B3} = 9$, respectively. Without loss of generality, the per dimension variance of dual-Rayleigh fading channels is set to $\Omega_v = 3$. We assume that the normalized distances between BS and CHVs are set as $d_{B1} = 0.5$, $d_{B2} = 0.7$ and $d_{B3} = 1$, respectively. The normalized distance between CHVs are set as $d_{12} = 0.5$, $d_{23} = 0.5$, respectively. The path loss factor is set as $\alpha = 3$.

Fig. 5 and Fig. 6 illustrate the convergence of the proposed algorithm in Case I and Case II, respectively. As expected, it converges fast to the optimal power allocation coefficient about a few iterations, because power allocation coefficients a_1^2, a_2^2 and a_3^2 only need the interval selection to be obtained quickly. Obviously, the numerical simulation results are consistent with the analysis values. Moreover, the

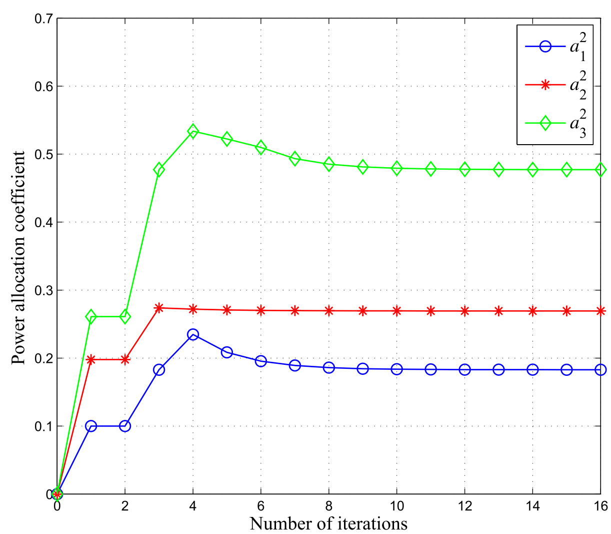

FIGURE 5. The convergence of the proposed algorithm in Case I.

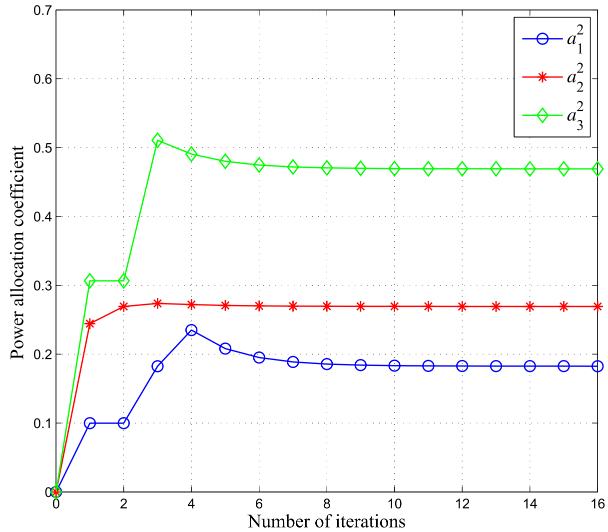

FIGURE 6. The convergence of the proposed algorithm in Case II.

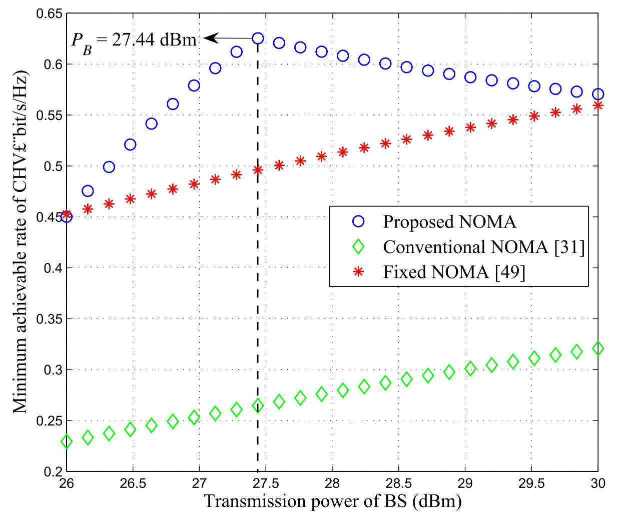

FIGURE 8. Minimum achievable rate of CHV under different transmission power of BS in Case II.

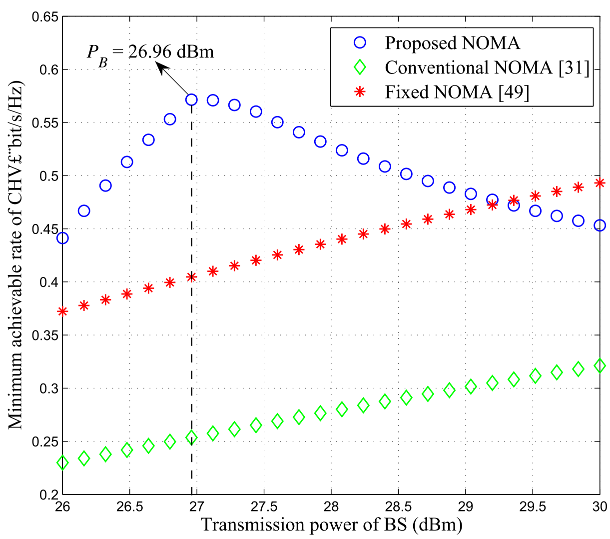

FIGURE 7. Minimum achievable rate of CHV under different transmission power of BS in Case I.

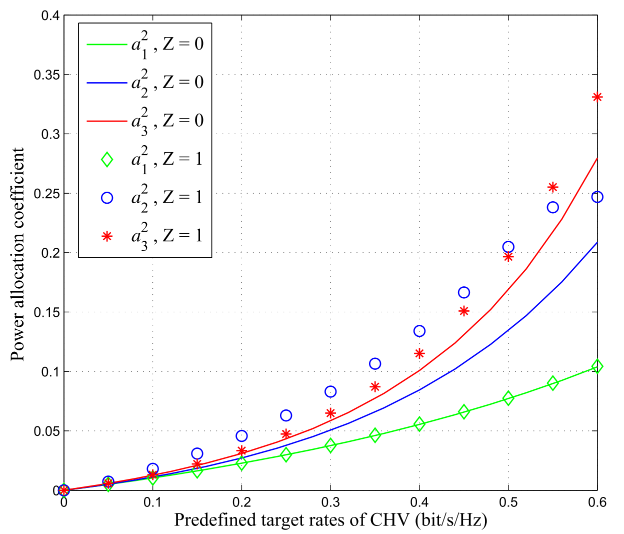

FIGURE 9. Power allocation coefficient versus different predefined target rates of CHV.

iterative calculation of the power allocation coefficient a_2^2 always converges fastest compared to the iterative calculation of the power allocation coefficient a_1^2 and a_3^2 which implies that the proposed scheme gives priority to the power allocation of the relay CHV for achieving better cooperative gain performance.

Fig. 7 plots the minimum achievable rate of CHV among three NOMA schemes under different transmission power of BS in Case I, where CHV-2 receives only the directly transmitted information from BS. We can observe that the minimum achievable rate of the proposed scheme is higher than that of the conventional NOMA scheme [31] and fixed NOMA scheme [49]. Moreover, it can be seen that the minimum achievable rate of the proposed scheme increases first and then decreases as the transmission power of BS increases. The reason is that the transmission power of the BS is increased to ensure that the CHV-2 was successful in receiving the information. Once the power allocation coefficient a_2^2 no longer increases, his results in a reduction in its achievable transmission rate. It is worth noting that we can find the extreme point (i.e., $P_B = 26.96$ dBm, $C_i = 0.5715$ bit/s/Hz) which maximizes the minimum achievable rate under low transmission power of BS.

Fig. 8 illustrates the minimum achievable rate of CHV under different transmission power of BS in Case II, where CHV-2 successfully receives the cooperative information from CHV-1. In this case, we can observe that the blue curve corresponding to the proposed scheme has also an extreme point (i.e., $P_B = 27.44$ dBm, $C_i = 0.6253$ bit/s/Hz). It also confirms that the proposed scheme not only can save the BS transmission power but also maximize the minimum achievable rate of CHV. Moreover, the minimum achievable rate of CHV has been increased compared to Case I. This highlights the cooperative performance gain of link CHV-1→CHV-2, with only a small quantity of transmission power of BS being sacrificed. Under the same conditions of P_B, the minimum achievable rate performance of the proposed NOMA scheme outperforms the conventional NOMA and fixed NOMA schemes.

Fig. 9 shows the variation of power allocation coefficient under different predefined target rates of CHV. In both cases, it can be seen that the three CHVs' power allocation coefficients gradually increase as the predefined target rates of CHV increase, where we must ensure that three CHVs' achievable rates are higher than their predefined target rates. In Case II, CHV-2 has obtained a cooperative gain from CHV-1. The power allocation coefficient a_2^2 exhibits a slow growth and thus reduces the transmission power of BS, while the power allocation coefficient a_3^2 keeps increasing due to poor channel quality of BS→CHV-3. Moreover, compared with Case I, the power allocation coefficients a_2^2 and a_3^2 are always larger than that of Case I, this is because the transmission power of BS is sacrificed in exchange for cooperative gain performance so as to increase the minimum transmission rate of CHV.

V. CONCLUSION

In this paper, we have proposed the joint clustering method and power control scheme in V2X communications to reduce the communication complexity as well as the total power consumption of BS. The proposed clustering method can not only dynamically adjust the cluster size according to actual traffic and road conditions, but also select out the CHVs with an optimal trade-off between the vehicle's relative speed and the transmission power. Numerical simulation results have showed the consistency with the analytical values. Furthermore, a NOMA-based power control scheme has been proposed to maximize the minimum achievable rate among CHV for a given transmission power of BS. Numerical simulation results have illustrated that the proposed power control scheme can significantly improve the achievable rate of CHV compared with the other two schemes (conventional NOMA and fixed NOMA) under the same transmission power of BS. These results prove the superiority performance of the proposed scheme. It lays the foundation for the research on clustering car-following V2X communication system, and has great practical value in vehicular networks.

APPENDIX

Proof of proposition 1: According to formula (46), using the Lagrange function is

$$\begin{aligned}
L\left(a_i^2, \alpha_i, \beta_i\right) &= a_1^2 + a_2^2 + a_3^2 + \alpha_1\left(2^{2\theta} - 1 - a_1^2 \frac{P_B|h_{B1}|^2}{N_0}\right) \\
&\quad + \alpha_2\left[2^{2\theta} - 1 - a_2^2\left(\frac{P_B|h_{B2}|^2}{a_1^2 P_B|h_{B2}|^2 + N_0}\right)\right]^{1-Z} \\
&\quad \times \left[2^{2\theta} - 1 - a_2^2 (c+d)\right]^Z \\
&\quad + \alpha_3\left[2^{2\theta} - 1 - a_3^2 (m+n)^{1-Z} \cdot (p+q)^Z\right] \\
&\quad - \sum\nolimits_{i=1}^{3} \beta_i \cdot a_i^2, \qquad (58)
\end{aligned}$$

where $\alpha_i \geq 0$ and $\beta_i \geq 0$ are the Karush-Kuhn-Tucker (KKT) multipliers [51]. According to KKT conditions, we can obtain

$$\frac{\partial L}{\partial a_1^2} = 1 - \alpha_1 \frac{P_B|h_{B1}|^2}{N_0} - \beta_1 = 0, \qquad (59)$$

$$\begin{aligned}
\frac{\partial L}{\partial a_2^2} &= 1 - \alpha_2\left(\frac{P_B|h_{B2}|^2}{a_1^2 P_B|h_{B2}|^2 + N_0}\right)^{1-Z} \\
&\quad \times (c+d)^Z - \beta_2 = 0, \qquad (60)
\end{aligned}$$

$$\frac{\partial L}{\partial a_3^2} = 1 - \alpha_3 (m+n)^{1-Z} \cdot (p+q)^Z - \beta_3 = 0, \qquad (61)$$

$$\beta_i \cdot a_i^2 = 0, \quad i = 1, 2, 3, \qquad (62)$$

$$\alpha_1\left(2^{2\theta} - 1 - a_1^2 \frac{P_B|h_{B1}|^2}{N_0}\right) = 0, \qquad (63)$$

$$\begin{aligned}
&\alpha_2\left(2^{2\theta} - 1 - a_2^2 \frac{P_B|h_{B2}|^2}{a_1^2 P_B|h_{B2}|^2 + N_0}\right)^{1-Z} \\
&\quad \times \left[2^{2\theta} - 1 - a_2^2 (c+d)\right]^Z = 0, \qquad (64)
\end{aligned}$$

$$\alpha_3\left[2^{2\theta} - 1 - a_3^2 (m+n)^{1-Z} \cdot (p+q)^Z\right] = 0, \qquad (65)$$

$$2^{2\theta} - 1 - a_1^2 \frac{P_B|h_{B1}|^2}{N_0} \leq 0, \qquad (66)$$

$$\begin{aligned}
&\left(2^{2\theta} - 1 - a_2^2 \frac{P_B|h_{B2}|^2}{a_1^2 P_B|h_{B2}|^2 + N_0}\right)^{1-Z} \\
&\quad \times \left[2^{2\theta} - 1 - a_2^2 (c+d)\right]^Z \leq 0, \qquad (67)
\end{aligned}$$

$$2^{2\theta} - 1 - a_3^2 (m+n)^{1-Z} \cdot (p+q)^Z \leq 0. \qquad (68)$$

It's obvious that $a_i^2 > 0$ $(i = 1, 2, 3)$, then we obtain $\beta_i = 0$ in the formula (62). Due to $\beta_i = 0$, $\alpha_i > 0$ can be derived from the equalities (59), (60) and (61). According to constraints (63), (64), (65) and $\alpha_i > 0$, the non-strict inequalities (66), (67) and (68) should take equal conditions, i.e., $C_i = \theta$ $(i = 1, 2, 3)$. The proof of the proposition 1 follows from these results.

REFERENCES

[1] T. Sahin, M. Klugel, C. Zhou, and W. Kellerer, "Virtual cells for 5G V2X communications," *IEEE Commun. Standards Mag.*, vol. 2, no. 1, pp. 22–28, Mar. 2018.

[2] C. Backfrieder, G. Ostermayer, and C. F. Mecklenbräuker, "Increased traffic flow through node-based bottleneck prediction and V2X communication," *IEEE Trans. Intell. Transp. Syst.*, vol. 18, no. 2, pp. 349–363, Feb. 2017.

[3] K. Lee, J. Kim, Y. Park, H. Wang, and D. Hong, "Latency of cellular-based V2X: Perspectives on TTI-proportional latency and TTI-independent latency," *IEEE Access*, vol. 5, pp. 15800–15809, 2017.

[4] R. Molina-Masegosa and J. Gozalvez, "LTE-V for sidelink 5G V2X vehicular communications: A new 5G technology for short-range vehicle-to-everything communications," *IEEE Veh. Technol. Mag.*, vol. 12, no. 4, pp. 30–39, Dec. 2017.

[5] S. Chen, J. Hu, Y. Shi, Y. Peng, J. Fang, R. Zhao, and L. Zhao, "Vehicle-to-everything (V2X) services supported by LTE-based systems and 5G," *IEEE Commun. Standards Mag.*, vol. 1, no. 2, pp. 70–76, Jun. 2017.

[6] H. Ullah, N. G. Nair, A. Moore, C. Nugent, P. Muschamp, and M. Cuevas, "5G communication: An overview of vehicle-to-everything, drones, and healthcare use-cases," *IEEE Access*, vol. 7, pp. 37251–37268, 2019.

[7] B. W. Khoueiry and M. R. Soleymani, "An efficient NOMA V2X communication scheme in the Internet of vehicles," in *Proc. VTC-Spring*, Sydney, NSW, Australia, Jun. 2017, pp. 1–7.

[8] C. B. Math, H. Li, S. H. de Groot, and I. G. Niemegeers, "V2X application-reliability analysis of data-rate and message-rate congestion control algorithms," *IEEE Commun. Lett.*, vol. 21, no. 6, pp. 1285–1288, Jun. 2017.

[9] H. Zhang, Y. Qiu, K. Long, G. K. Karagiannidis, X. Wang, and A. Nallanathan, "Resource allocation in NOMA-based fog radio access networks," *IEEE Wireless Commun.*, vol. 25, no. 3, pp. 110–115, Jun. 2018.

[10] Y. Zhou, V. W. S. Wong, and R. Schober, "Dynamic decode-and-forward based cooperative NOMA with spatially random users," *IEEE Trans. Wireless Commun.*, vol. 17, no. 5, pp. 3340–3356, May 2018.

[11] H. Zheng, H. Li, S. Hou, and Z. Song, "Joint resource allocation with weighted max-min fairness for NOMA-enabled V2X communications," *IEEE Access*, vol. 6, pp. 65449–65462, 2018.

[12] B. Di, L. Song, Y. Li, and Z. Han, "V2X meets NOMA: Non-orthogonal multiple access for 5G-enabled vehicular networks," *IEEE Wireless Commun.*, vol. 24, no. 6, pp. 14–21, Dec. 2017.

[13] B. Di, L. Song, Y. Li, and G. Y. Li, "Non-orthogonal multiple access for high-reliable and low-latency V2X communications in 5G systems," *IEEE J. Sel. Areas Commun.*, vol. 35, no. 10, pp. 2383–2397, Oct. 2017.

[14] X. Zhou and A. Boukerche, "AFLAS: An adaptive frame length aggregation scheme for vehicular networks," *IEEE Trans. Veh. Technol.*, vol. 66, no. 1, pp. 855–867, Jan. 2017.

[15] X. Zhang, X. Cao, L. Yan, and D. K. Sung, "A street-centric opportunistic routing protocol based on link correlation for urban vanets," *IEEE Trans. Mobile Comput.*, vol. 15, no. 7, pp. 1586–1599, Jul. 2016.

[16] V. Nguyen, O. T. T. Kim, C. Pham, T. Z. Oo, N. H. Tran, C. S. Hong, and E.-N. Huh, "A survey on adaptive multi-channel MAC protocols in VANETs using Markov models," *IEEE Access*, vol. 6, pp. 16493–16514, 2018.

[17] C. Cooper, D. Franklin, M. Ros, F. Safaei, and M. Abolhasan, "A comparative survey of vanet clustering techniques," *IEEE Commun. Surveys Tuts.*, vol. 19, no. 1, pp. 657–681, 1st Quart., 2017.

[18] J. R. Dawande, S. Silakari, and A. J. Deen, "Enhanced distributed multi-hop clustering algorithm for VANETs based on neighborhood follow (EDMCNF) collaborated with road side units," in *Proc. IEEE CICN*, Jabalpur, India, Dec. 2015, pp. 106–113.

[19] S. Y. Kannekanti, G. S. P. Nunna, V. K. R. Bobba, A. K. Yadama, and A. Elleithy, "An efficient clustering scheme in vehicular ad-hoc networks," in *Proc. IEEE UEMCON*, New York, NY, USA, Oct. 2017, pp. 282–287.

[20] F. Chiti, R. Fantacci, and G. Rigazzi, "A mobility driven joint clustering and relay selection for IEEE 802.11p/WAVE vehicular networks," in *Proc. IEEE ICC*, Sydney, NSW, Australia, Jun. 2014, pp. 348–353.

[21] S. Ucar, S. Ergen, and O. Ozkasap, "Multihop-cluster-based IEEE 802.11p and LTE hybrid architecture for VANET safety message dissemination," *IEEE Trans. Veh. Technol.*, vol. 65, no. 4, pp. 2621–2636, Apr. 2016.

[22] A. Abuashour and M. Kadoch, "Performance improvement of cluster-based routing protocol in VANET," *IEEE Access*, vol. 5, pp. 15354–15371, 2017.

[23] A. A. Khan, M. Abolhasan, and W. Ni, "An evolutionary game theoretic approach for stable and optimized clustering in VANETs," *IEEE Trans. Veh. Technol.*, vol. 67, no. 5, pp. 4501–4513, May 2018.

[24] J. Wang, K. Liu, K. Xiao, C. Chen, W. Wu, V. C. Lee, and S. H. Son, "Dynamic clustering and cooperative scheduling for vehicle-to-vehicle communication in bidirectional road scenarios," *IEEE Trans. Intell. Transp. Syst.*, vol. 19, no. 6, pp. 1913–1924, Jun. 2018.

[25] L. Liang, J. Kim, S. C. Jha, K. Sivanesan, and G. Y. Li, "Spectrum and power allocation for vehicular communications with delayed CSI feedback," *IEEE Wireless Commun. Lett.*, vol. 6, no. 4, pp. 458–461, Aug. 2017.

[26] Y. Ren, F. Liu, Z. Liu, C. Wang, and Y. Ji, "Power control in D2D-based vehicular communication networks," *IEEE Trans. Veh. Technol.*, vol. 64, no. 12, pp. 5547–5562, Dec. 2015.

[27] S. Guo and X. Zhou, "Robust power allocation for NOMA in heterogeneous vehicular communications with imperfect channel estimation," in *Proc. IEEE Annu. Int. Symp. PIMRC*, Montreal, QC, Canada, Oct. 2017, pp. 1–5.

[28] L. P. Qian, Y. Wu, H. Zhou, and X. Shen, "Dynamic cell association for non-orthogonal multiple-access V2S networks," *IEEE J. Sel. Areas Commun.*, vol. 35, no. 10, pp. 2342–2356, Oct. 2017.

[29] Y. Chen, L. Wang, Y. Ai, B. Jiao, and L. Hanzo, "Performance analysis of NOMA-SM in vehicle-to-vehicle massive MIMO channels," *IEEE J. Sel. Areas Commun.*, vol. 35, no. 12, pp. 2653–2666, Dec. 2017.

[30] J. Chen, L. Yang, and M.-S. Alouini, "Physical layer security for cooperative NOMA systems," *IEEE Trans. Veh. Technol.*, vol. 67, no. 5, pp. 4645–4649, May 2018.

[31] Z. Ding, M. Peng, and H. V. Poor, "Cooperative non-orthogonal multiple access in 5G systems," *IEEE Commun. Lett.*, vol. 19, no. 8, pp. 1462–1465, Aug. 2015.

[32] E. Okamoto, H. Okada, Y. Ishii, and S. Makido, "Performance improvement of low-latency V2I uplink using superposed cooperative V2V transmission," in *Proc. IEEE VTC-Fall*, Toronto, ON, Canada, Sep. 2017, pp. 1–5.

[33] S. Hao, L. Yang, and Y. Shi, "Data-driven car-following model based on rough set theory," *IET Intell. Transp. Syst.*, vol. 12, no. 1, pp. 49–57, Feb. 2018.

[34] B. Higgs and M. Abbas, "Segmentation and clustering of car-following behavior: Recognition of driving patterns," *IEEE Trans. Intell. Transp. Syst.*, vol. 16, no. 1, pp. 81–90, Feb. 2015.

[35] Y. Li, L. Zhang, H. Zheng, X. He, S. Peeta, T. Zheng, and Y. Li, "Nonlane-discipline-based car-following model for electric vehicles in transportation-cyber-physical systems," *IEEE Trans. Intell. Transp. Syst.*, vol. 19, no. 1, pp. 38–47, Jan. 2018.

[36] Y.-F. Shi, L.-C. Yang, S.-X. Hao, and Q. Liu, "Clustered car-following strategy for improving car-following stability under cooperative vehicles infrastructure systems," *IET Intell. Transp. Syst.*, vol. 10, no. 3, pp. 141–147, Apr. 2016.

[37] M. Rahman, M. Chowdhury, T. Khan, and P. Bhavsar, "Improving the efficacy of car-following models with a new stochastic parameter estimation and calibration method," *IEEE Trans. Intell. Transp. Syst.*, vol. 16, no. 5, pp. 2687–2699, Oct. 2015.

[38] Q. Wang, P. Fan, and K. B. Letaief, "On the joint V2I and V2V scheduling for cooperative vanets with network coding," *IEEE Trans. Veh. Technol.*, vol. 61, no. 1, pp. 62–73, Jan. 2012.

[39] R. Protzmann, B. Schunemann, and I. Radusch, "The influences of communication models on the simulated effectiveness of V2X applications," *IEEE Commun. Mag.*, vol. 49, no. 11, pp. 149–155, Nov. 2011.

[40] P. S. Bithas, G. P. Efthymoglou, and A. G. Kanatas, "V2V cooperative relaying communications under interference and outdated CSI," *IEEE Trans. Veh. Technol.*, vol. 67, no. 4, pp. 3466–3480, Apr. 2018.

[41] T. T. Duy, G. C. Alexandropoulos, V. T. Tung, V. N. Son, and T. Q. Duong, "Outage performance of cognitive cooperative networks with relay selection over double-Rayleigh fading channels," *IET Commun.*, vol. 10, no. 1, pp. 57–64, 2016.

[42] Y. Liu, Z. Qin, M. Elkashlan, Y. Gao, and L. Hanzo, "Enhancing the physical layer security of non-orthogonal multiple access in large-scale networks," *IEEE Trans. Wireless Commun.*, vol. 16, no. 3, pp. 1656–1672, Mar. 2017.

[43] Z. Ding, Y. Liu, J. Choi, Q. Sun, M. Elkashlan, C.-L. I, and H. V. Poor, "Application of non-orthogonal multiple access in LTE and 5G networks," *IEEE Commun. Mag.*, vol. 55, no. 2, pp. 185–191, Feb. 2017.

[44] H. Xiao, Y. Hu, K. Yan, and S. Ouyang, "Power allocation and relay selection for multisource multirelay cooperative vehicular networks," *IEEE Trans. Intell. Transp. Syst.*, vol. 17, no. 11, pp. 3297–3305, Nov. 2016.

[45] A. Chelli, E. Zedini, M. S. Alouini, M. Pätzold, and I. Balasingham, "Throughput and delay analysis of HARQ with code combining over double Rayleigh fading channels," *IEEE Trans. Veh. Technol.*, vol. 67, no. 5, pp. 4233–4247, May 2018.

[46] Z. Zhang, Z. Ma, M. Xiao, Z. Ding, and P. Fan, "Full-duplex device-to-device aided cooperative non-orthogonal multiple access," *IEEE Trans. Veh. Technol.*, vol. 66, no. 5, pp. 4467–4471, May 2017.

[47] Y. Alghorani, G. Kaddoum, S. Muhaidat, S. Pierre, and N. Al-Dhahir, "On the performance of multihop-intervehicular communications systems over n*Rayleigh fading channels," *IEEE Wireless Commun. Lett.*, vol. 5, no. 2, pp. 116–119, Apr. 2016.

[48] S. Timotheou and I. Krikidis, "Fairness for non-orthogonal multiple access in 5G systems," *IEEE Signal Process. Lett.*, vol. 22, no. 10, pp. 1647–1651, Oct. 2015.

[49] Z. Ding, P. Fan, and H. V. Poor, "Impact of user pairing on 5G nonorthogonal multiple-access downlink transmissions," *IEEE Trans. Veh. Technol.*, vol. 65, no. 8, pp. 6010–6023, Aug. 2016.

[50] P. Wang, B. Di, H. Zhang, K. Bian, and L. Song, "Cellular V2X communications in unlicensed spectrum: Harmonious coexistence with VANET in 5G systems," *IEEE Trans. Wireless Commun.*, vol. 17, no. 8, pp. 5212–5224, Aug. 2018.

[51] F.-S. Tseng, C.-T. Lin, and W.-R. Wu, "Optimum transceiver designs in two-hop amplify-and-forward MIMO relay systems with SIC receivers," *IEEE Trans. Veh. Technol.*, vol. 64, no. 3, pp. 985–997, Mar. 2015.

HAILIN XIAO (M'15) received the B.S. degree from Wuhan University, in 1998, the M.S. degree from Guangxi Normal University, in 2004, and the Ph.D. degree from the University of Electronic Science and Technology of China (UESTC), in 2007. He was a Research Fellow with the School of Engineering and Physical Sciences, Joint Research Institute for Signal and Image Processing, Heriot-Watt University, from 2011 to 2012. He was also a Research Fellow with the School of Electronics and Computer Science (ECS), University of Southampton, from 2016 to 2017. He is currently a Professor with the School of Computer Science and Information Engineering, Hubei University, China. He has published one book chapter and over 200 papers in refereed journals and conference proceedings. His research interests include MIMO wireless communications, cooperative communications, and vehicular communication.

Dr. Xiao has served as a TPC Member and a Session Chair for some international conferences. He received the Guangxi Natural Science Foundation for Distinguished Young Scholars, the Guangxi Natural Science Award, and the Distinguished Professor of the Qianjiang Scholars, China, in 2014, 2015, and 2018, respectively.

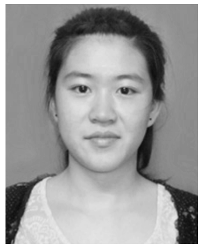

YUHONG CHEN received the B.S. degree from the Changchun University of Technology (CCUT), China, in 2016. She is currently pursuing the Ph.D. degree with the Guilin University of Electronic Technology (GUET), China.

Her research interests include vehicular cooperative communications and power allocation.

SHAN OUYANG (M'02–SM'09) received the B.S. degree in electronic engineering from the Guilin University of Electronic Technology, China, in 1986, and the M.S. and Ph.D. degrees in electronic engineering from Xidian University, Xi'an, China, in 1992 and 2000, respectively. From 2001 to 2002, he was a Research Associate with the Department of Electronic Engineering, The Chinese University of Hong Kong. From 2003 to 2004, he was a Research Fellow with the Department of Electronic Engineering, University of California at Riverside. He is currently a Professor with the School of Information and Communications, Guilin University of Electronic Technology (GUET), China. His research interests are mainly in the areas of signal processing for communications and radar, adaptive filtering, and neural network learning theory and applications. He received the Outstanding Youth Award of the Ministry of Electronic Industry and Guangxi Province Outstanding Teacher Award, China, in 1995 and 1997, respectively. He received the National Excellent Doctoral Dissertation of China, in 2002.

ANTHONY THEODORE CHRONOPOULOS (M'87–SM'98) received the Ph.D. degree in computer science from the University of Illinois at Urbana–Champaign, in 1987. He is currently a Professor in computer science with The University of Texas at San Antonio. He is also a Visiting Faculty Member with the Department of Computer Engineering and Informatics, University of Patras. He has published 68 journal and 71 refereed conference proceedings publications in the areas of distributed systems, high-performance computing, and applications. He is a Fellow of the Institution of Engineering and Technology (IET) and an ACM Senior Member. He has been awarded 15 federal/state government research grants. He has 2100 non-self-citations and h-index of 29.